Research paper

Modification of Axial Distribution of Fragment Velocity in Preformed Fragmentation Warheads

Xin Li[1,2,*], Weili Wang[1], Zhengfeng Liang[2], Jun Dong[3]

[1] *Naval University of Engineering, China*
[2] *Xi'an Modern Chemistry Research Institute, China*
[3] *Xi'an Jiaotong University, China*
* E-mail: syhshanxi2008@126.com

Abstract: Fragment velocity is a crucial parameter for evaluating the destructive capability of a warhead, and it is typically calculated using the Gurney formula with corrections. The currently established correction formulas can determine the axial distribution of natural fragment velocity within the shell, but for a preformed fragmentation warhead, energy losses due to the existence of fragment gaps lead to calculated results that are larger than the actual values, making it unsuitable for accurate calculation of the axial distribution of fragment velocity in such warheads. This paper introduces a filling ratio correction function based on the concept of effective charge and establishes a calculation model for the axial distribution of fragment velocity in preformed fragmentation warheads. The numerical simulation method was validated using prototype ground static explosion test data, then the influence of key parameters such as charge diameter (*d*), length-diameter ratio (*δ*), and filling ratio (*β*) on the axial distribution of fragment velocity was investigated. The relationships between the three parameters (*a*, *m*, *c*) in the filling ratio correction function and the characteristic parameters were derived, and the filling ratio correction function and the calculation formula for the axial distribution of fragment velocity were fitted. Comparisons with existing empirical formulas indicate that the formulas established in this paper offer higher calculation accuracy, with an error of no more than 4.65% compared to measured values, and they can reliably determine the axial distribution of fragment velocity in preformed fragmentation warheads, providing significant practical application value.

Keywords: preformed fragmentation warhead, velocity, length-diameter ratio, filling ratio, calculation formula

1 Introduction

Fragments are one of the main destructive elements of fragmentation warheads, and generate impact damage on targets through high-speed projection by explosive driving. Based on the fragment generation process, they can be classified into natural, semi-preformed, and preformed fragments. Under the same charge structure of a warhead, the driving time of fragments caused by detonation loading varies. Among the three types of fragments, natural fragments are subjected to detonation loading for the longest time, followed by semi-preformed fragments, and preformed fragments have the shortest driving time. As a result, this leads to significant differences in the initial velocity of the three types of fragments under the same detonation loading condition [1-3]. While fragment velocity is one of the key parameters for evaluating the lethality of fragments, accurate calculation of fragment velocities for different types of fragments is of significant guiding importance in effectively assessing the damage effects of fragments on military objectives or targets and in constructing a damage power field model of warheads.

Researchers have conducted extensive studies on fragment velocity and established many semi-empirical and semi-theoretical calculation formulas. The most typical one is the initial velocity formula of fragments based on the energy distribution proposed by Gurney [4], which assumes that all parts of the cylindrical shell rupture under the same stress and the resulting fragments have the same initial velocity along the axis of the cylindrical shell. This formula is applicable for the natural fragments generated by a cylindrical shell and can be expressed as:

$$v_0 = \sqrt{2E} / \sqrt{\frac{1}{\beta} + 0.5} \tag{1}$$

where v_0 and $\sqrt{2E}$ are the initial casing velocity and the Gurney velocity, respectively. In addition, β represents the filling ratio, which is the ratio of the explosive mass to the casing mass.

In fact, due to the limited length of the shell, there is a rarefaction wave effect at both ends of the explosive charge, resulting in different velocities of fragments along the same axis. Typically, the maximum velocity is located at the axial center, while it decreases at the sides due to the influence of the rarefaction wave effects [5-10]. In order to accurately predict the velocities of fragments near both ends of the shell, researchers have developed modified formulas for the axial distribution of fragment velocities considering the effects of rarefaction waves at

both ends based on the Gurney formula. One approach involves modifying the filling ratio based on the Gurney formula. Charran [11] eliminated the velocity influence of the rarefaction waves at both ends by adjusting the filling ratio. This researcher proposed an innovative method based on the principle of effective charge, wherein a cone is removed from each end of the cylindrical charge, with the height of the initiation end cone equal to the diameter of the charge, and the height of the non-initiation end cone equal to the radius of the charge. Subsequently, a formula for calculating the velocity of fragments for the case of end-face initiation was established, and the formula takes the following form:

$$v(x) = \frac{\sqrt{2E}}{\sqrt{\left(\frac{1}{\beta f(x)} + 0.5\right)}} \tag{2}$$

In the Equation 2, $f(x) = 1 - \left[1 - min\left(\frac{x}{2r}, 1, \frac{L-x}{r}\right)\right]^2$, where x represents the distance from the initiation point at the end, r is the charge radius, and L is the charge length.

In addition, another method is to add a correction function in the Gurney formula. Zulkouski [12] conducted experimental research on the axial distribution characteristics of natural fragment velocities under an end-face initiation condition of an internal explosive loaded in a cylindrical metal shell. This study focused on the end-face rarefaction wave effect. By fitting the experimental data, a modified Gurney formula considering the rarefaction wave effect was proposed to predict the axial initial velocities of fragments. Felix [13] proposed a rapid calculation model for the axial distribution of natural fragment velocities in cylindrical shells initiated at the end-face point based on previous experimental data. Feng [14] and Huang [15] used pulse X-ray to test the axial distribution of natural fragment velocities for cylindrical shells under end-face initiation. By fitting the experimental data to the Gurney formula, an empirical formula for the axial distribution of natural fragment velocities for warheads was established. Based on this empirical formula, they further derived calculation formulas for warheads with center initiation, which is expressed as Equation 3.

$$v(x) = \left[1 - 0.3615e^{-1.111\frac{x}{d}}\right]\left[1 - 0.3615e^{-1.111\frac{L-x}{d}}\right]\sqrt{2E}\sqrt{\frac{\beta}{1+0.5\beta}} \tag{3}$$

where d is the charge diameter.

Furthermore, considering the variations in the structural shell, the characteristics of axial fragment velocity distribution will be altered [16-18]. For non-cylindrical shells, Guo *et al.* [16] utilized flash photography techniques to study the velocity distribution of fragments along the axis under end-face initiation. The results indicated that the rarefaction wave generated at both ends of the non-cylindrical shells were only related to the explosive diameter, not the filling ratio. Based on these conclusions, an "effective charge" equivalent model was proposed, and its parameters were determined by analyzing the velocity distribution of different charge cases. This equation can directly generate the velocity distribution of non-cylindrical casings initiated at one end without the need to experimentally determine unknown parameters.

Based on the above analysis, it can be concluded that current research mainly focuses on the axial distribution of natural fragment velocities generated in cylindrical or non-cylindrical shells, while there is still a lack of study on the axial distribution of fragment velocities from preformed shells. Taking into account that the energy losses caused by the escape of detonation gases from the preformed fragment gaps, utilizing the established empirical formula for natural fragment velocities to calculate velocities from preformed shells would lead to overestimation and is not suitable for solving preformed fragment velocities. Therefore, a correction factor is typically added to the Gurney formula to calculate preformed fragment velocities, with a common value of 0.9 [19]. However, this approximate value is not accurate, and is generally considered to provide a reasonable estimate for fragment velocities at the axial center, but produces large errors for fragment velocities at other positions.

In the present paper, we introduce a filling ratio correction function and propose a theoretical model of the axial distribution of fragment velocities in preformed fragmentation warheads initiated at the center, built upon the effective charge. The validation of the numerical simulation method was performed through ground static explosion test data from principle prototypes. Subsequently, the numerical simulation method was employed to investigate the influence of characteristic parameters, such as charge diameter, length-diameter ratio and filling ratio, on the axial distribution of fragment velocities. A filling ratio correction function was fitted to obtain the modified Gurney formula. Finally, the accuracy of the proposed formula was verified.

2   Computational Model

In response to the influence of the rarefaction wave effect on the axial distribution of fragment velocity under end point initiation, one reference [11] proposed the concept of the effective charge, achieving preliminary calculations of the axial distribution of fragment velocities by deliberately altering the filling ratios at the initiation end and the non-initiation end. However, the main issue with this approach is the lack of a theoretical basis and experimental data in support for the removal of explosive. Specifically, the typical problem was the near-zero mass of the effective charge at both ends after removal, resulting in zero fragment velocities at the ends calculated using the Gurney formula, which did not align with actual test data. Nonetheless, the idea of altering local filling ratios through segmented interior explosive cutting is highly meaningful. Inspired by this method, the axial velocity distribution of preformed fragments initiated at the center was investigated.

The theoretical model of the effective charge for a preformed fragment warhead initiated at the center is shown in Figure 1. The warhead consists of charge, preformed fragments, front end plate, rear end plate and liner. The charge length is L, the charge diameter is d, the charge radius is r, the fragment thickness is t, and I is the initiation point. In practical applications, considering that the primary function of the end plates and the liner is to form a sealed cavity for the charge and the preformed fragments; thin-walled components are generally selected for them, with thicknesses of 5 and 1 mm, respectively. The explosive was divided into effective charge (highlighted in red) and ineffective charge (highlighted in gray). The effective charge is further divided into three areas: Region I, Region II, and Region III.

For Region I, according to relevant experimental results [6, 20, 21], the maximum fragment velocity occurs at the axial center under center point initiation. As the warhead length is increased, the fragment velocity near the axial center is basically the same, *i.e.* the filling ratio and effective charge mass are the same, respectively. Therefore, there is no rarefaction wave effect in the central region. Meanwhile, based on cylindrical explosion tests, the expansion ratio of the cylindrical shell when gas leakage first occurs ranges from 1.6 to 2.1, depending on the type of explosive filling. However, for a cylindrical shell made with preformed fragments, gas leakage occurs at an expansion ratio of 1.18 to 1.26. This indicates that most of the energy escapes between the fragments without contributing to their acceleration. Consequently, Region I contains ineffective charge represented by the gray section, assuming an ineffective charge radius of c corresponding to an axial length of l.

For Regions II and III, the fragment velocity is completely symmetrical, and it is affected by both the rarefaction wave and the energy loss due to the gaps between fragments. The closer to the end, the greater the influence of the rarefaction wave on the fragments, resulting in a more pronounced velocity decrease. At the warhead ends, the fragment velocity is the lowest. Hence, the gray section of ineffective charge in the two end regions is larger than that in the intermediate Region I. Moreover, it is assumed that the ineffective charge radius varies linearly along the axis direction, with the end ineffective charge radius being "*m*", and the axial length affected by the rarefaction wave leading to a velocity decrease being "*a*".
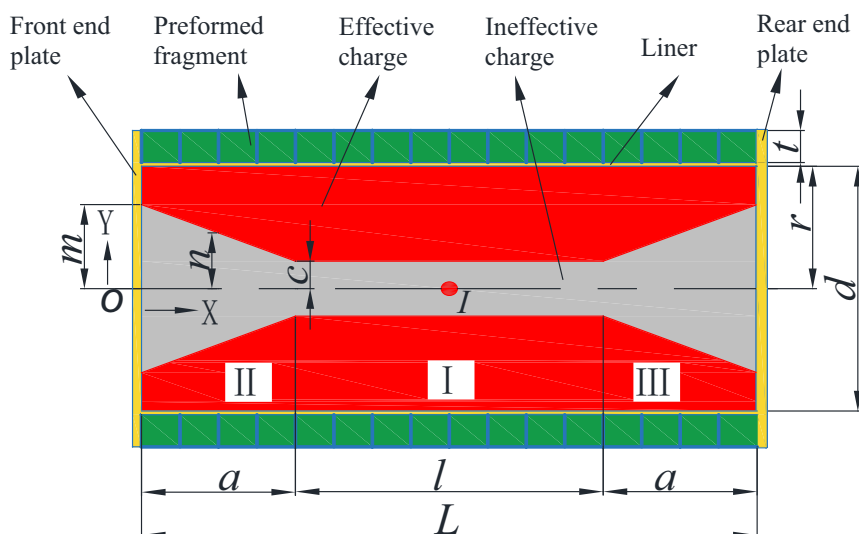

Figure 1.   Theoretical model of the effective charge

The filling ratios of the three regions are calculated below, where the filling ratio correction function for Region I is constant and expressed as:

$$F(x) = \frac{\pi r^2 - \pi c^2}{\pi r^2} = 1 - \left(\frac{c}{r}\right)^2 \tag{4}$$

Due to the similarity between Region II and Region III, Region II is taken as an example to calculate the filling ratio correction functions at both ends. Firstly, a coordinate system with the center of the charge as the origin O is established. Based on geometric relationships, the removed charge radius n at a distance x from point O satisfies the following Equation 5:

$$\frac{n\text{-}c}{m\text{-}c}=\frac{a\text{-}x}{a}=1-\frac{x}{a} \tag{5}$$

Since the filling ratio is related to the charging structure, the correction function is the ratio of the charging mass after removal to the charging mass before removal. Therefore, the filling ratio correction function for Region II is:

$$F(x)=\frac{\pi r^2\text{-}\pi n^2}{\pi r^2}=1-\left[\frac{(1\text{-}x/a)(m\text{-}c)+c}{r}\right]^2 \tag{6}$$

When $x = 0$, the terminal correction function is:

$$F(x)=\frac{\pi r^2\text{-}\pi m^2}{\pi r^2}=1-\left(\frac{m}{r}\right)^2 \tag{7}$$

Based on Equations 4, 6, and 7, it is evident that the filling ratio correction function for Region I is only related to parameter c, while the filling ratio correction function for Region II depends on parameters a, m, and c. Specifically, the correction function for the end of Region II is solely related to parameter m. Hence, the following parameters are determined separately for a, m, and c.

For a centrally initiated explosive warhead, the characteristic parameters are the charge diameter d, length-diameter ratio δ, and filling ratio β, all of which may influence parameters a, m, and c. Therefore, a, m, and c are expressed in the following forms:

$$a = f(d, \delta, \beta) \tag{8}$$

$$m = f(d, \delta, \beta) \tag{9}$$

$$c = f(d, \delta, \beta) \tag{10}$$

To determine the expressions of the above three parameters, a single-factor control variable method is employed, utilizing numerical simulations to investigate the influence of the characteristic parameters on the three parameters, respectively.

3   Numerical Simulation

The numerical simulation for the axial velocity of preformed fragments under explosive detonation loading were performed by the LS-DYNA dynamic simulation software. The calculation model for a preformed fragmentation warhead is shown in Figure 2, and consists of preformed fragments, charge, liner, front and rear end plates. The warhead diameter and length are 112 and 210 mm, respectively, and the charge diameter and length are 100 and 200 mm, respectively. The round is configured with 20 axial rings, each containing 31 fragments, for a total of 620 tungsten alloy fragments. The fragment size is 10×10×5 mm. For modelling, the front and rear end plates, liner, and fragments of the warhead were represented using a single-point-integrated Lagrange hexahedral grid, and a Lagrange algorithm was used for the elements. The explosive was modelled using a Euler hexahedral grid, with a single-point Euler algorithm utilized for the elements. The three-dimensional fluid-solid coupling Multi-Material Arbitrary Lagrangian-Eulerian (MMALE) algorithm with single-layer mesh was employed for coupling calculations. The air boundary was treated with a non-reflecting free boundary condition. The mesh size was set to 0.5 mm, and the modelling was performed in the cm-g-µs unit system.
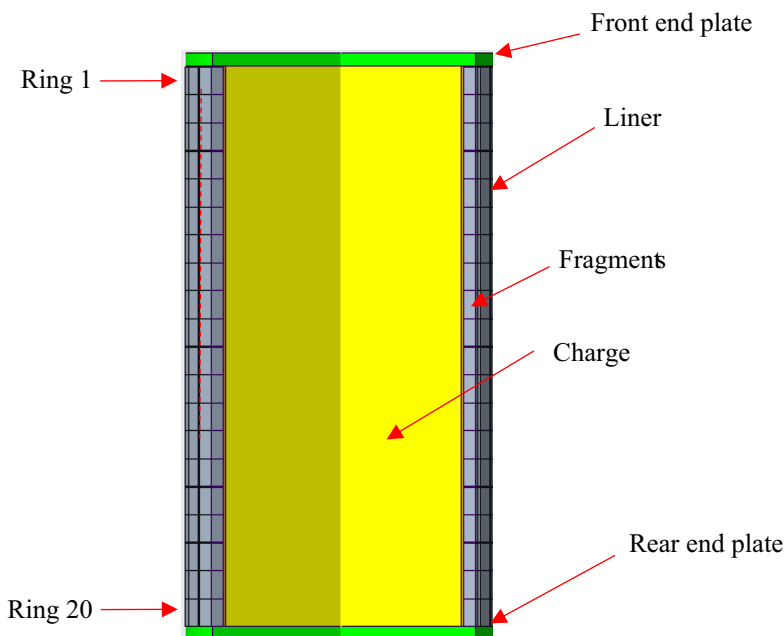

Figure 2.   Numerical calculation model

The explosive used in this study was HMX-based Plastic-Bonded Explosive (PBX), with the main components being 62% HMX, 18% Al, 9% binder, and 11% other additives. The explosive behaviour was described using both the JWL state equation and the MAT_HIGH_EXPLOSIVE_BURN detonation model. The JWL state equation is an empirical equation determined from experimental data, which can accurately describe the pressure, energy, and volume expansion characteristics of detonation products during the detonation driving process. The expression of the JWL state equation is as follows:

$$p = A\left(1 - \frac{\omega}{R_1 V}\right)\exp(-R_1 V) + B\left(1 - \frac{\omega}{R_2 V}\right)\exp(-R_2 V) + \frac{\omega E}{V} \tag{11}$$

where V represents the specific volume of the detonation products and E denotes the initial internal energy of the explosive. A, B, R_1, R_2 and ω are constants that characterize the detonation properties of the explosive. The material parameters for the explosive are listed in Table 1 [22]. The fragments are made of tungsten alloy and modelled using the PLASTIC_KINEMATIC kinematic hardening model, with the corresponding parameters listed in Table 2 [23].

Table 1.   HMX-based PBX explosive material parameters

ρ [kg·m^{-3}]	P_{CJ} [GPa]	D [m·s^{-1}]	A [GPa]	B [GPa]	R_1	R_2	ω
1818	31.86	8336	748.6	13.38	4.5	1.2	0.38

Table 2.   Material parameters of tungsten alloy

ρ [kg·m^{-3}]	E [GPa]	G [GPa]	μ	σ_y [GPa]	n
17.6	357	7.9	0.303	2	1

The front and rear end plates, as well as the liner, are all made of 2A12 aluminum alloy, and are described using a combination of the Johnson-Cook constitutive model and the Gruneisen state equation, which can effectively capture the strain hardening, thermal softening, and damage accumulation effects of the materials. The fracture in the Johnson-Cook material model is characterized by the cumulative damage parameter D, and failure occurs when $D = 1$, resulting in a removal of the material element. The material parameters for 2A12 aluminum alloy are listed in Table 3 [24]. The expansion and fragmentation process of the preformed fragment under explosive driving is shown in Figure 3.

Table 3. Material parameters of 2A12 aluminum alloy

Johnson-Cook constitutive model							
ρ [kg·m^{-3}]	E [GPa]	μ	A' [MPa]	B' [MPa]	n	C'	m
2760	68.96	0.33	265	426	0.34	0.15	1.0
Gruneisen state equation							
S		C [m·s^{-1}]			γ		
1.338		5328			2.0		

$t = 0$ μs

$t = 5$ μs

$t = 25$ μs

$t = 50$ μs

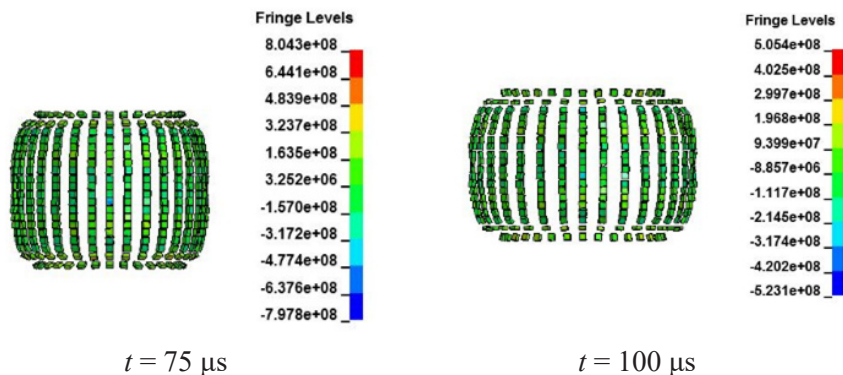$t = 75$ µs $t = 100$ µs
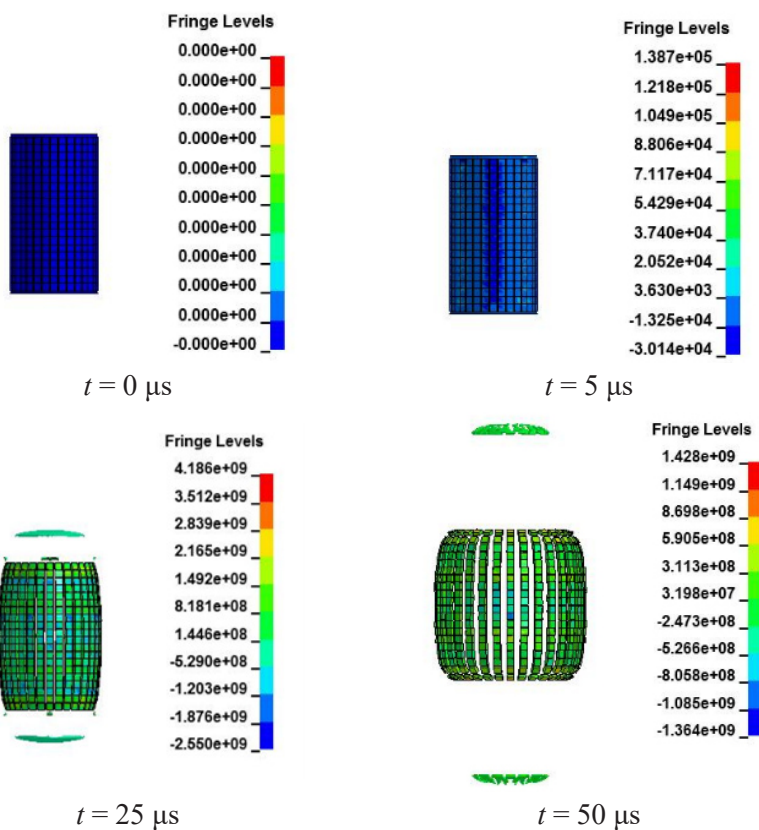
Figure 3.   Numerical simulation results of the fragment driving process

     As shown in Figure 3, it can be observed that the fragments near the central detonation experience radial expansion initially. In the axial direction, due to the influence of the rarefaction wave, the fragment velocity at the axial center is significantly higher than that of the fragments at both ends. The results of the axial distribution of fragment velocities obtained from the numerical simulation are shown in Table 4.

Table 4.   Numerical simulation results of axial fragment velocity distribution

Ring	Fragment velocity [m·s⁻¹]	Ring	Fragment velocity [m·s⁻¹]
1	915.9	11	1668.6
2	1056.1	12	1596.4
3	1189.5	13	1588.7
4	1259.8	14	1500.4
5	1386.8	15	1458.5
6	1456.0	16	1388.4
7	1502.0	17	1262.3
8	1589.2	18	1184.9
9	1595.6	19	1055.4
10	1668.6	20	916.8

4   Experimental Verification

In order to verify the accuracy of numerical simulations, an experiment was performed to investigate the velocity distribution of preformed fragments.

A prototype was designed and fabricated based on the simulation model, and the total mass of the warhead was approximately 9.0 kg. Fragments were made of tungsten alloy having size 10×10×5 mm and arranged in a brick pattern on a 1 mm thick aluminum casing (density 2.7 g/cm³) using a resin hardener mix. Each fragment had a mass of 8.75 g. The charge used in the prototype was HMX-based PBX high-energy explosive, with a charge mass of 2.63 kg and filling ratio of 0.484. In the warhead the detonator extended to the center position through a hollow tube to achieve center point initiation. The hollow tube was made of organic glass and had a diameter of only 10 mm, which had a negligible impact on the filling ratio. The prototype is shown in Figure 4.

A schematic diagram of the experimental layout is shown in Figure 5. Specifically, Q235A steel plates with an arc length of 20 m and a height of 4m were placed at a power radius of 6 m. Meridian and latitude lines were drawn on the target plates, with the vertical centerline of the target plate as the reference at 90°, and vertical lines were drawn every 3150 mm (30°) on the left and right sides. The latitude line was drawn every 210 mm (2°) on the horizontal centerline as the reference at 0°. Off targets were placed along the power radius at 1, 2, 3, 4 and 5 m in three directions of 230°, 270° and 310°, respectively, which were used to measure the velocity attenuation coefficient of the fragments. High-speed photography was conducted at a frame rate of 10,000 frames per second (fps).
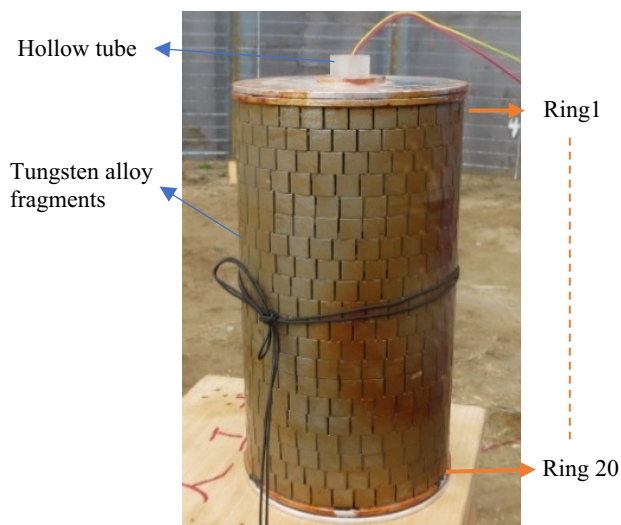

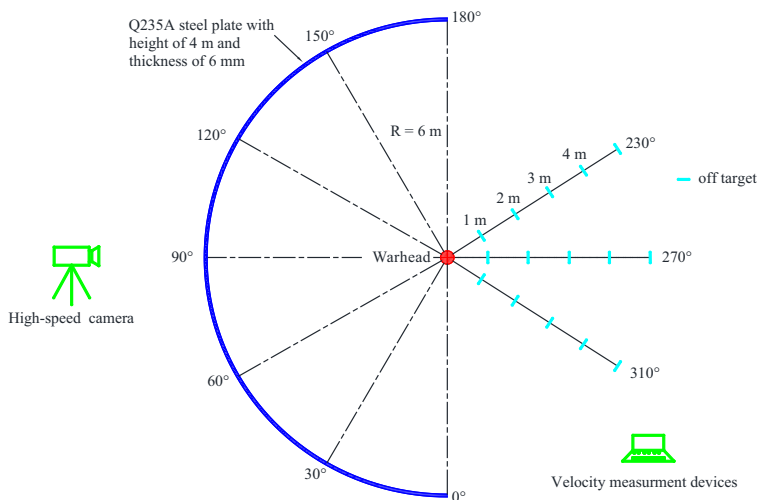**Figure 4.**   Preformed fragmentation warhead prototype

Figure 5.   Schematic diagram of experimental layout

Through different off target tests, the time taken for fragments to reach various distances was measured. Subsequently, in accordance with GJB5232.3-2004 "*Test method for arena of tactical missile warhead performances - Part 3: Determination of fragment initial velocity in fixed point explosion test*", the fragment velocity attenuation coefficient α was calculated, which can be expressed as:

$$\alpha = \frac{\sum_{i=1}^{N} S_i \cdot \sum_{i=1}^{N} \ln V_i - n \sum_{i=1}^{N} S_i \ln V_i}{N \sum_{i=1}^{n} S_i^2 - (\sum_{i=1}^{n} S_i)^2} \tag{12}$$

where i is target number, $N = 5$, S_i is distance from the detonation center to the midpoint between adjacent targets, V_i is average velocity of fragments between adjacent target, which can be expressed respectively as:

$$S_i = R_{i-1} + \frac{R_i - R_{i-1}}{2} \tag{13}$$

$$V_i = \frac{R_i - R_{i-1}}{T_i - T_{i-1}} \tag{14}$$

where R_i is the distance from the detonation center to the i-th target, T_i is the flight time of the fragment from the detonation center to the i-th target.

The fragment velocity attenuation coefficient was calculated to be 0.022, as shown in Table 5. Figure 6 illustrates the detonation moments of the warhead prototype and the instants when fragments penetrated the steel plates at different axial positions. The moment when the warhead detonates and forms a firelight was taken as the starting time.

Table 5. Calculation results of the fragment attenuation coefficient

i	R_i [m]	S_i [m]	T_i [ms]	T_i [m·s^{-1}]	α
1	1	0.50	0.60	1666.67	
2	2	1.50	1.25	1538.46	
3	3	2.50	1.95	1428.57	0.022
4	4	3.50	2.70	1333.33	
5	5	4.50	3.50	1250.00	

(a) $t = 0$ ms, Initiation of warhead

(b) $t = 3.8$ ms, Rings 9~12 fragments

(c) $t = 4.0$ ms, Rings 6~15 fragments

(d) *t* = 4.2 ms, Rings 5~16 fragments

(e) *t* =4.6 ms, Rings 4~17 fragments

(f) *t* = 5.2 ms, Rings 1~20 fragments

Figure 6.   Light generated as fragments penetrated the steel plate at different axial positions

It can be seen from Figure 6 that the fragments at the axial center penetrate the target first, producing a bright flash of light at 3.8 ms. Subsequently, the luminous phenomenon gradually extends towards both ends, with the end fragments exhibiting the longest illumination time and the lowest velocity. The axial distribution of fragment velocities was obtained by converting the captured fireball generated after the fragments penetrated the steel plates using the high-speed camera. Utilizing the previously obtained fragment velocity attenuation coefficient, the fragment velocity at typical axial positions was derived according to Equation 15, where v_x is the instantaneous velocity of fragments at 3 m, which is approximately equal to the average velocity of fragments within 6 m.

$$v_0 = \frac{v_x}{e^{-\alpha \cdot x}} \tag{15}$$

From this, it can be concluded that the fragment velocity of ring 9 to ring 12 near the equatorial plane was the highest, at 1686.7 m/s, the fragment velocity of ring 6 and ring 15 was 1526.0 m/s, the fragment velocity of the ring 5 and ring 16 was 1456.7 m/s, the fragment velocity of the ring 4 and ring 17 was 1323.3 m/s, and the fragment velocity of ring 1 and ring 20 was 890.2 m/s. A comparison between the experimental results and the numerical results is shown in Figure 7.
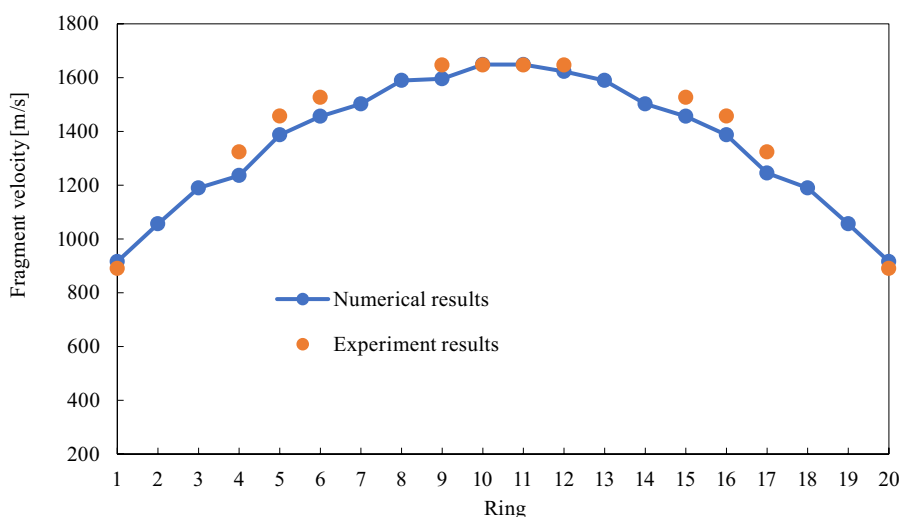

Figure 7. Comparison between numerical simulation values and test values

From Figure 7, it became evident that the fragment velocity exhibits a symmetrical normal distribution relative to the equatorial plane. The maximum fragment velocity, defined as "v_{max}", occurred near the axial center. The numerical simulation yielded a peak fragment velocity of 1668.6 m/s, while the experimental value recorded 1686.7 m/s, a deviation of approximately –1.1%. Due to the influence of the rarefaction wave, the end fragments experienced the lowest velocity, designated as "v_{min}". The numerical simulation indicated a minimum fragment velocity of 915.9 m/s, while the experimental value was 890.2 m/s, resulting in an error of about 2.8%. The maximum error in other positions was –4.1%, demonstrating a good agreement between the numerical results and the experimental values, thereby affirming the accuracy of the numerical simulation method in predicting the axial distribution of fragment velocity.

5   Results and Discussion

5.1 Effects factor analysis

5.1.1 Effect of charge diameter

In order to investigate the impact of charge diameter on the axial distribution characteristics of fragment velocity, the charge diameter was considered as the sole variable while keeping the filling ratio and length-diameter ratio constant. Table 6 lists the structural parameters of a warhead with nine different charge diameters, along with the numerical simulation results of the maximum fragment velocity at the axial center and the minimum fragment velocity at both ends. Additionally, Figure 8 illustrates the trends of fragment velocity distribution under various working conditions.

Table 6.   Structural parameters of a warhead with different charge diameters and maximum/minimum fragment velocities at axial positions

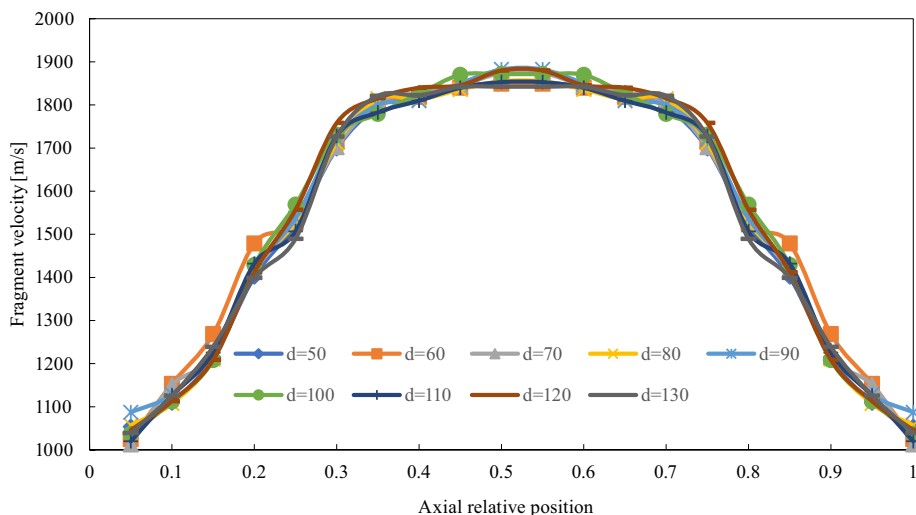| No.	Charge length L [mm]	Charge diameter d [mm]	Fragment thickness t [mm]	δ	β	Fragment velocity	
						v_{max} [m·s^{-1}]	v_{min} [m·s^{-1}]
1	100	50	1.70			1852.3	1053.5
2	120	60	2.04			1849.2	1024.7
3	140	70	2.38			1864.2	1012.4
4	160	80	2.72			1854.7	1056.8
5	180	90	3.06	2	0.723	1862.3	1086.9
6	200	100	3.40			1871.3	1036.8
7	220	110	3.74			1852.9	1019.9
8	240	120	4.08			1859.8	1045.8
9	260	130	4.42			1842.3	1038.9

Figure 8.   Axial distribution of fragment velocity for different charge diameters

In Table 6 and Figure 8, it is noticeable that as the filling ratio and length-diameter ratio remain constant and only the charge diameter is changed, the axial distribution of fragment velocity remains nearly identical. Moreover, the fragment velocities at different positions are essentially consistent. This indicates that when the warhead dimensions are proportionally increased or decreased, the axial distribution trend of the fragment velocity is the same, suggesting the absence of a scale effect.

5.1.2 *Effect of length-diameter ratio*
In order to study the effect of the length-diameter ratio on the axial distribution characteristics of fragment velocity, the length-diameter ratio was set as the sole variable while keeping the filling ratio and charge diameter constant. Table 7 gives the structural parameters of a warhead with ten different length-diameter ratios, along with the numerical simulation results for the maximum fragment velocity at the axial center and the minimum fragment velocity at both ends. Furthermore, Figure 9 illustrates the trends of fragment velocity distribution at various axial positions under different working conditions.

Table 7. Structural parameters of a warhead with different length-diameter ratios and the maximum/minimum fragment velocities at axial positions

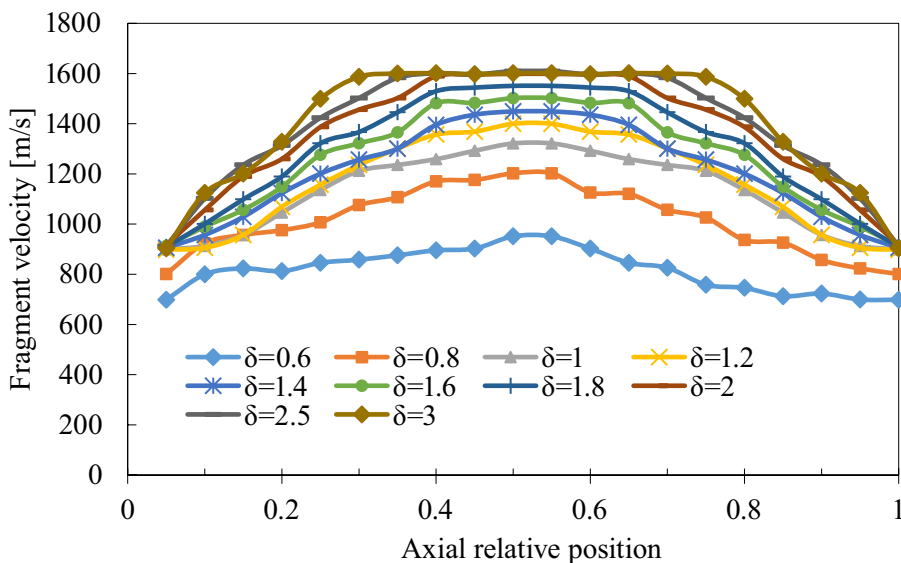| No.	Charge length L [mm]	Charge diameter d [mm]	Fragment thickness t [mm]	δ	β	Fragment velocity	
						v_{max} [m·s⁻¹]	v_{min} [m·s⁻¹]
1	60	100	5	0.6		951.2	698.5
2	80	100	5	0.8		1202.4	801.1
3	100	100	5	1.0		1321.4	899.4
4	120	100	5	1.2		1399.8	898.2
5	140	100	5	1.4	0.497	1448.7	905.6
6	160	100	5	1.6		1501.9	912.7
7	180	100	5	1.8		1550.7	908.6
8	200	100	5	2.0		1598.6	915.9
9	250	100	5	2.5		1609.2	920.7
10	300	100	5	3		1601.3	918.9

Figure 9. Axial distribution of fragment velocity at different length-diameter ratios

From Table 7 and Figure 9, it is evident that the length-diameter ratio has a significant impact on the distribution of fragment velocity along the axial direction. When δ is small, the fragment velocity distribution curve exhibits

a „⌒„ shape. On the other hand, when δ is large, the curve presents a „⌒„ shape. Moreover, with further increase of δ, the detonation becomes more complete, leading to a longer plateau period. This indicates that a higher proportion of fragments reach maximum velocity along the axial direction. Regarding the fragment velocity at the axial center, when $\delta \leq 2$, a larger length-diameter ratio results in a higher fragment velocity. However, when $\delta \geq 2$, the fragment velocity at the axial center remains relatively constant, allowing for the neglect of the influence of rarefaction waves at both ends on the velocity. This finding aligns with previous research [25] on the impact of δ on fragment velocity in the equatorial plane. As for the fragment velocity at the end faces, when $\delta \geq 1$, the velocity is basically relatively constant, indicating that the length-diameter ratio has little effect. However, when $\delta < 1$, smaller ratios lead to lower fragment velocities.

5.1.3 Effect of filling ratio

In order to figure out the impact of the filling ratio on the axial distribution characteristics of the fragment velocity, while the length-diameter ratio δ and the charge diameter d are kept unchanged; β was set as the only variable. Table 8 provides the structural parameters of nine different warheads with varying filling ratios and the corresponding numerical simulation results for the maximum fragment velocity and the minimum fragment velocity at different axial positions. Figure 10 shows the axial distribution trend of fragment velocity under different working conditions.

Table 8. Structural parameters of projectiles with different filling ratios and maximum/minimum fragment velocities at axial positions

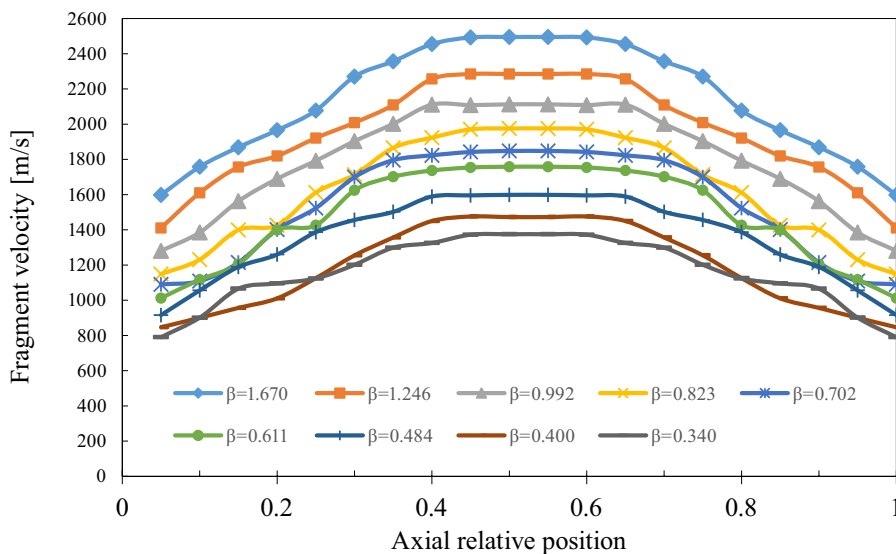| No.	Charge length L [mm]	Charge diameter d [mm]	Fragment thickness t [mm]	δ	β	Fragment velocity	
						v_{max} [m·s^{-1}]	v_{min} [m·s^{-1}]
1	200	100	1.5		1.670	2495.1	1598.1
2	200	100	2		1.246	2285.2	1410.8
3	200	100	2.5		0.992	2112.7	1280.7
4	200	100	3		0.823	1975.6	1148.6
5	200	100	3.5	22	0.702	1847.8	1090.0
6	200	100	4		0.611	1758.3	1012.5
7	200	100	5		0.484	1600.7	915.9
8	200	100	6		0.400	1472.5	846.7
9	200	100	7		0.340	1375.1	790.2

Figure 10. Axial distribution of fragment velocity at different filling ratios

It can be observed from Table 8 and Figure 10 that the trend of fragment velocity distribution at axial positions under different filling factors is basically the same. The distribution curve presents a „⌒„ shape, and the length of the plateau period is basically the same. Simultaneously, the ratio between the minimum velocity at both ends and the maximum velocity at the equatorial plane ranges from 0.57 to 0.64, indicating that the filling ratio has little influence on the axial distribution of fragment velocity.

5.2 Correction function and calculation formula

5.2.1 Calculation of c and m

Based on the numerical simulation results of axial fragment velocity distribution under different charge diameters, length-diameter ratios and filling ratios, combined with the theoretical model formulas, *i.e.* Equations 4 and 7, the relationships between c/r, m/r, and d, δ, β can be derived. The curves depicting these relationships are shown in Figures 11-13.
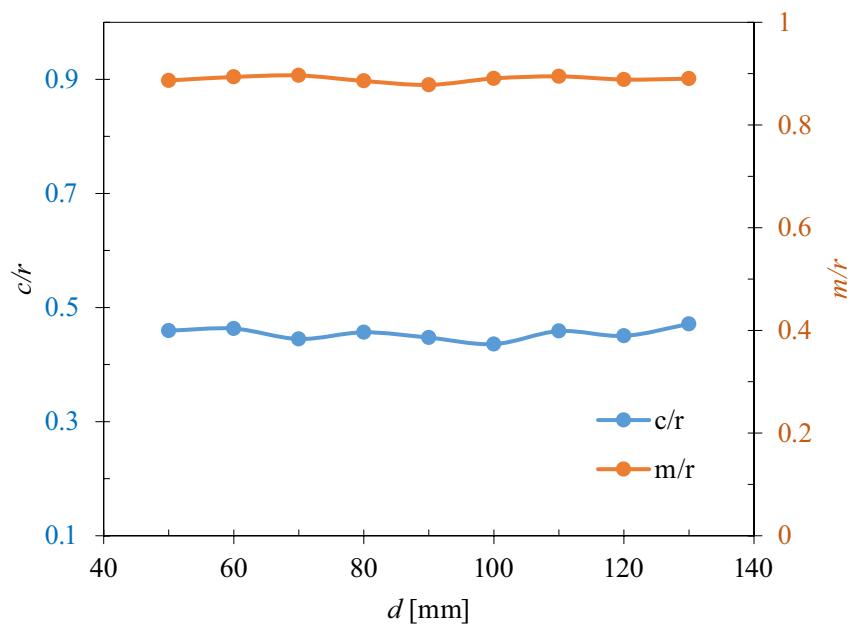
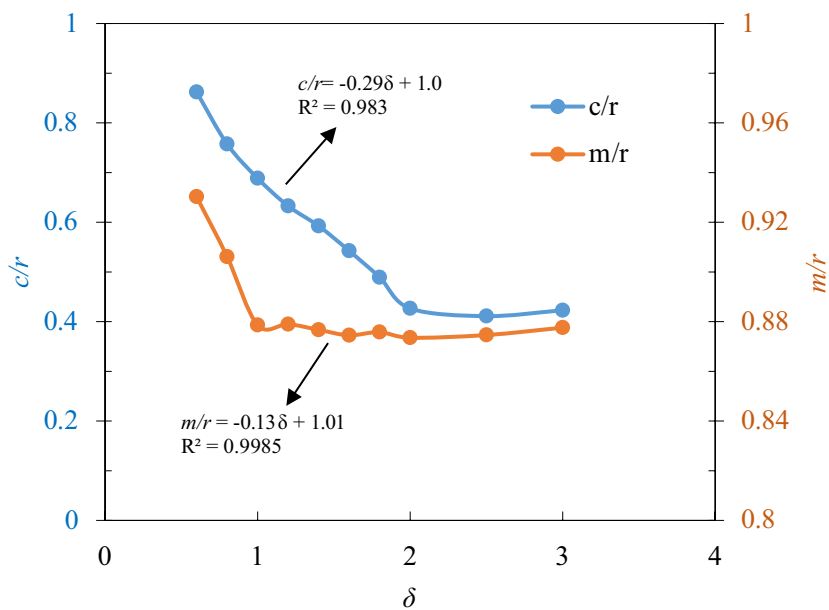**Figure 11.** Relationship curves of *c*/*r* and *m*/*r* with charge diameter

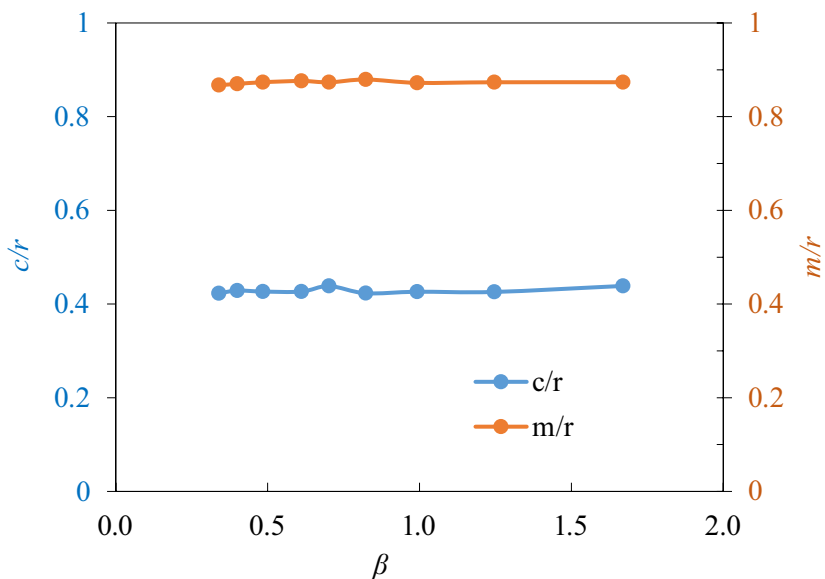**Figure 12.** Relationship curves of *c*/*r* and *m*/*r* with length-diameter ratio

Figure 13. Relationship curves of *c/r* and *m/r* with filling ratio

It can be observed that *c/r* and *m/r* are independent of charge diameter and filling ratio, remaining constant, as shown in Figures 11 and 13. By contrast, Figure 12 shows that *c/r* and *m/r* are closely related to the length-diameter ratio. For *c/r*, when $\delta \leq 2$, *c/r* exhibits an approximately linear relationship with δ, with a fitting correlation coefficient of 0.983. When $\delta \geq 2$, *c/r* becomes constant. For *m/r*, when $\delta \leq 1$, the relationship between m/r and δ is approximately linear, with a fitting correlation coefficient of 0.9985. When $\delta \geq 1$, *m/r* is constant.

5.2.2 Calculation of a

According to the numerical simulation results of axial fragment velocity distribution under different charge diameters, length-diameter ratios and filling ratios, the relationship between *a/L* and *d*, δ, β can be obtained as shown in Figures 14-16.
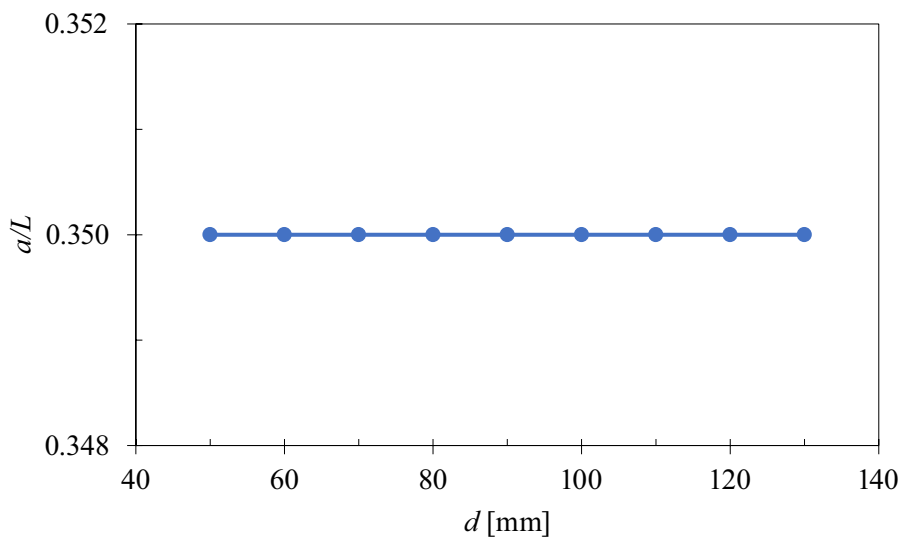
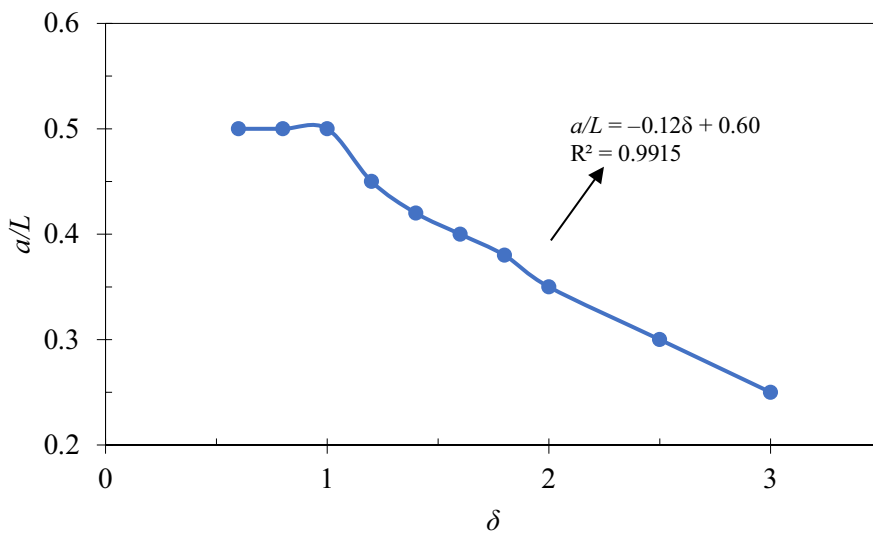**Figure 14.** Relationship curve of a/L with charge diameter

Figure 15. Relationship curve of a/L with length-diameter ratio
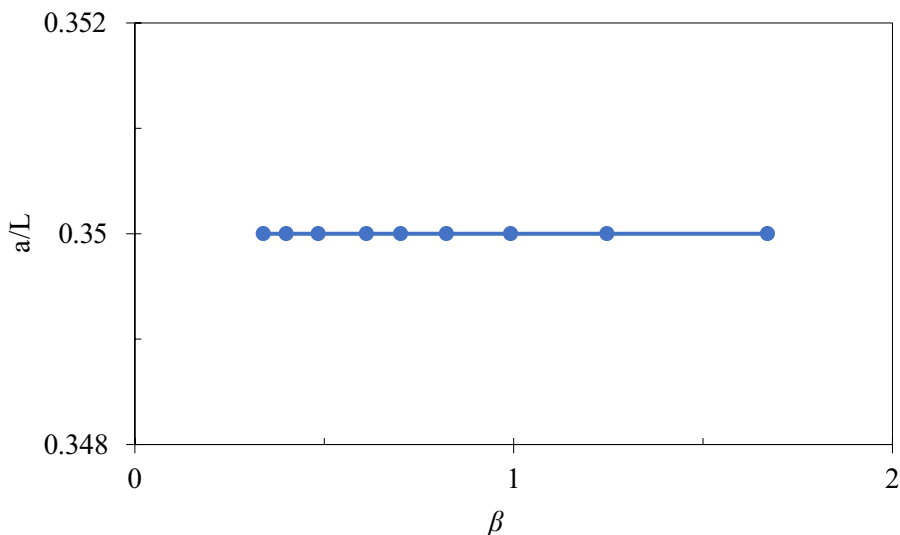
Figure 16. Relationship curve of a/L with filling ratio

As can be seen from Figures 14 and 16, it is noticeable that a/L is independent of charge diameter and filling ratio, remaining constant. However, Figure 15 reveals that when $\delta \leq 1$, the axial length a affected by rarefaction waves accounts for half of the total length L, that is that all fragments along the axial direction are influenced by rarefaction waves. When $\delta \geq 1$, a/L gradually decreases with an increasing length-diameter ratio and shows an approximately linear relationship with δ, with a correlation coefficient of 0.9915. When the value of δ reaches 2, the axial length a affected by rarefaction waves comprises 36% of the total length L. Therefore, for the design of fragment warhead structures, it is preferable to maximize the length-diameter ratio.

5.2.3 Calculation Formula and discussion

As seen from the results presented in Sections 5.2.1 and 5.2.2, it is evident that the length-diameter ratio has a significant influence on c, m, and a, while the influence of the filling ratio and the charge diameter can be neglected. Accordingly, the corresponding correction functions for the effective charge in different regions can be given as follows:

–   for Region I, the correction function expression is:

$$F(x, \ \delta) = \begin{cases} 1-(-0.29\delta+1.0)^2, & \delta \leq 2 \\ 0.82, & \delta > 2 \end{cases} \tag{16}$$

– for Region II or Region III, the correction function expression is:

$$F(x,\ \delta)=\begin{cases} 1-\left[\left(1-\frac{x}{0.5L}\right)(0.16\delta+0.01)+(-0.29\delta+1.0)\right]^2, & \delta<1 \\ 1-\left[\left(1-\frac{x}{L(-0.12\delta+0.60)}\right)(0.29\delta-0.12)+(-0.29\delta+1.0)\right]^2, & 1\leq\delta\leq2 \quad (17) \\ 1-\left[\left(1-\frac{x}{L(-0.12\delta+0.60)}\right)0.46+0.42\right]^2, & \delta>2 \end{cases}$$

Applying the function $F(x, \delta)$ to the Gurney formula, the expression for the axial distribution of fragment velocity can be obtained:

$$v(x) = \sqrt{2E}\Big/\sqrt{\frac{1}{\beta F(x,\ \delta)}+0.5} \qquad (18)$$

When using the above formula, initially calculate the axial length *a* influenced by rarefaction waves based on the given length-diameter ratio. Then, based on this, divide the charge part into Region I, Region II, and Region III, and subsequently apply the filling ratio correction functions of Region I, Region II, and Region III to the Gurney formula to obtain the axial fragment velocity distribution results when the center point of the preformed fragmentation warhead is initiated.

To assess the accuracy of the proposed formula, the axial fragment velocity distribution of the prototype was calculated by using the formula established in this paper. The results were then compared and analyzed against the experimental data. Additionally, the calculated values were compared with those obtained from the Gurney Equation 1 and the natural fragment velocity empirical Equations 2 and 3. These results are shown in Figure 17.
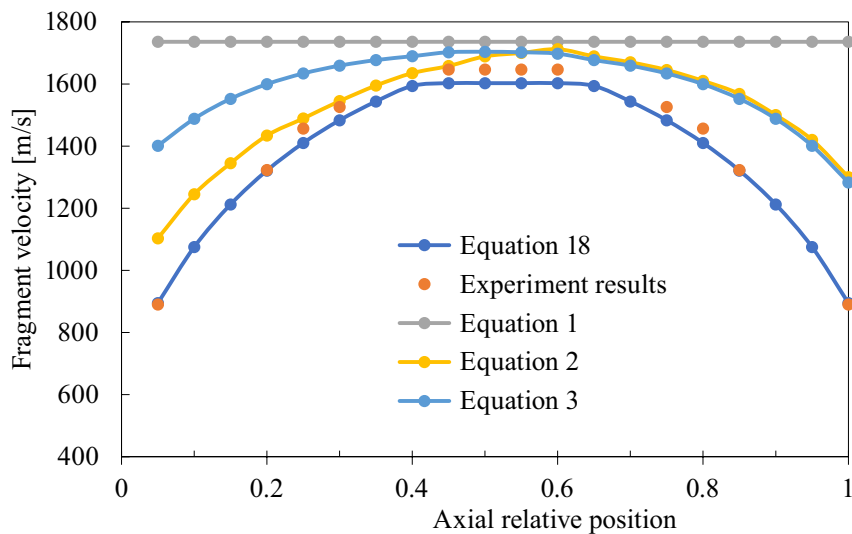
Figure 17. Comparison of the results of the calculated fragment velocities with experimental results, and values from existing formulas

Figure 17 demonstrates a strong agreement between the calculated values derived from the proposed formula and the experimental results, with a maximum deviation of only 4.65% at different positions. This indicates that the computational model established in this paper is accurate, enabling the determination of the axial fragment velocity distribution under different working conditions for a preformed fragmentation warhead initiated at the center. On the other hand, for the currently available natural fragment velocity empirical formula, the calculated values at different positions are consistently higher than the experimental results, especially at the two ends, with a difference of up to 35.7%. The reason for this discrepancy is that the natural fragment velocity calculation model is based on the results of spontaneous fragmentation tests of the charge detonation in the shell. As mentioned earlier, the explosive radius of preformed fragmentation warheads is smaller than that of the shell's expansion radius, resulting in a lower impulse from the explosive detonation products and relatively lower fragment velocities. Moreover, closer to the ends, this difference is more significant. Therefore, when using the Gurney formula to calculate fragment velocities, the structural form of the warhead's fragments must be considered. In order to analyze further, the calculated fragment velocities at different axial positions were divided by the Gurney formula's calculated results, resulting in axial fragment velocity correction factors, as shown in Figure 18.
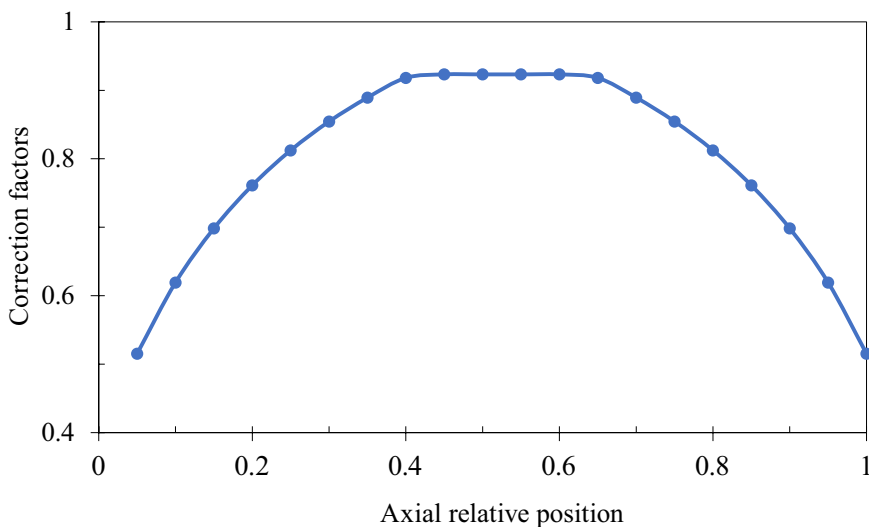
Figure 18. Fragment velocity correction factors at different axial positions

As deduced from Figure 18, the correction factor is not a constant value, ranging from 0.515 to 0.923. The maximum value of 0.923 is found near the equatorial plane, and the minimum value of 0.515 is found at the edges. This further illustrates that when using the Gurney formula to calculate fragment velocities for a preformed fragmentation warhead, a coefficient value of 0.9 is reasonable for the equatorial plane. However, for other axial positions, especially those close to the ends, a coefficient value of 0.9 is evidently higher than the actual correction needed.

6   Conclusions

This study investigated the axial distribution of fragment velocities for preformed fragmentation warheads initiated at the center, discussed the influence of rarefaction waves and energy loss in the gaps between preformed fragments on the axial velocity distribution of fragments, and introduced a filling ratio correction function based on the concept of effective charge. Consequently, a calculation formula for the axial fragment velocity distribution of a preformed fragmentation warhead was proposed. The effects of charge diameter, length-diameter ratio, and filling ratio on the fragment velocity distribution were systematically studied by a numerical simulation method, which was experimentally verified. The following main conclusions were drawn:

♦ There is energy loss in the gaps between the preformed fragments, which significantly impacts the axial fragment velocity distribution. Under the same working conditions, the axial velocity of the fragment is lower than that of a natural fragment.

♦ Based on the concept of effective charge, the explosive charge can be divided into three regions. The central region (Region I) is affected by energy loss due to the fragment gaps, while the two end regions (Region II and Region III) are influenced by both rarefaction waves and energy loss from the fragment gaps. The filling ratio correction functions corresponding to each region are closely related to the length-diameter ratio and independent of the charge diameter and the filling ratio. As the length-diameter ratio increases, the ratio of the axial length affected by the rarefaction waves to the total length decreases.

♦ A calculation formula for the axial fragment velocity distribution of a preformed fragmentation warhead initiated at the center was established. Compared to experimental data, the formula yielded an error within 4.65%, and showed higher accuracy when compared to existing formulas for calculating natural fragment velocities. The formula can be applied to calculate the axial velocities of preformed fragments under different charge diameters, length-diameter ratios, and filling ratios when initiated at the center. This can guide the design of preformed fragmentation warhead structures and assess their lethal performance.

References

[1] Martineau, R.L.; Anderson, C.A.; Smith, F.W. Expansion of Cylindrical Shells Subjected to Internal Explosive Detonations. *Exp. Mech.* **2000**, *20*: 219-225; https://doi.org/10.1007/BF02325049.

[2] Hutchinson, M.D. The Escape of Blast from Fragmenting Munitions Casings. *Int. J. Impact Eng.* **2009**, *36*: 185-192; https://doi.org/10.1016/j.ijimpeng.2008.05.002.

[3] Li, X.; Wang, W.; Liang, Z. Research Progress on Acceleration Ability of Explosive Detonation to Metal Shell. *J. Projectiles, Rockets, Missiles and Guidance* **2022**, *42*: 7-14.

[4] Gurney, R.W. *The Initial Velocities of Fragments from Bombs, Shells and Grenades.* Report No 405, Ballistic Research Laboratories (BRL), Aberdeen Proving Ground, USA-MD, **1943**.

[5] Karpp, R.R.; Predebon, W.W. *Calculations of Fragment Velocities from Naturally Fragmenting Munitions.* Report No 2509, Ballistic Research Laboratories (BRL), Aberdeen Proving Ground, USA-MD, **1975**.

[6] Szmelter, J.; Davies, N.; Lee, C.K. Simulation and Measurement of Fragment Velocity in Exploding Shells. *J. Battlefield Technol.* **2007**, *10*: 1-7.

[7] Hu, N.; Zhu, X.; Chen, C. Theoretical Calculation of the Fragment Initial Velocity Following Aerial Explosion of the Cylindrical Warhead with Two Terminals. *IOP Conf.* **2017**, *274*: 1-8.

[8] Hennequin, E. Influence of the Edge Effects on the Initial Velocity of Fragments from a Warhead. *Proc. 9th Int. Symp. Ballistics*, Shrivenham, UK, **1986**.

[9] Randers, P.G. An Improved Equation for Calculating Fragment Projection Angles. *Proc. 2nd Int. Symp. Ballistics*, Daytona Beach, USA, **1976**.

[10] Grisaro, H.; Dancygier, A.N. Numerical Study of Velocity Distribution of Fragments Caused by Explosion of a Cylindrical Cased Charge. *Int. J. Impact. Eng.* **2015**, *86*: 1-12; https://doi.org/10.1016/j.ijimpeng.2015.06.024.

[11] Charron, Y.J. *Estimation of Velocity Distribution of Fragmenting Warheads Using a Modified Gurney Method*. Report ADA074759, Air Force Inst. of Tech. Wright-Pattersonafb Oh School of Engineering, USA-OH, **1979**, pp. 113-116.

[12] Zulkowski, T. *Development of Optimum Theoretical Warhead Design Criteria.* Report No AD-B015617, Naval Weapons Center, China Lake, USA-CA, **1976**.

[13] Felix, D.; Colwill, I.; Stipidis, E. Real-time Calculation of Fragment Velocity for Cylindrical Warheads. *Def. Technol.* **2019**, *15*: 264-271; https://doi.org/10.1016/j.dt.2019.01.007.

[14] Feng, S.; Cui, B. An Experimental Investigation for the Axial Distribution of Initial Velocity of Shells. *Acta Armamentarii* **1987**, *4*: 60-63.

[15] Huang, G.; Li, W.; Feng, S. Axial Distribution of Fragment Velocities from Cylindrical Casing under Explosive Loading. *Int. J. Impact Eng.* **2015**, *76*: 20-27; https://doi.org/10.1016/j.ijimpeng.2014.08.007.

[16] Guo, Z.; Huang, G.; Liu, C. Velocity Axial Distribution of Fragments from Non-cylindrical Symmetry Explosive-filled Casing. *Int. J. Impact Eng.* **2018**, *118*: 1-10; https://doi.org/10.1016/j.ijimpeng.2018.03.011.

[17] Liao, W.; Jiang, J.; Men, J. Effect of the End Cap on the Fragment Velocity Distribution of a Cylindrical Cased Charge. *Def. Technol.* **2021**, *17*: 1052-1061; https://doi.org/10.1016/j.dt.2020.06.024.

[18] Gao, Y.; Feng, S.; Yan, X. Axial Distribution of Fragment Velocities from Cylindrical Casing with Air Parts at Two Ends. *Int. J. Impact Eng* **2020**, *140*: 103535-103545; https://doi.org/10.1016/j.ijimpeng.2020.103535.

[19] Lloyd, R.M. *Conventional Warhead Systems Physics and Engineering Design.* Virginia 1: American Institute of Aeronautics and Astronautics, **1998**.

[20] Jaansalu, K.M.; Dunning, M.R. Fragment Velocities from Thermobaric Explosives in Metal Cylinders. *Propellants, Explos. Pyrotech.* **2007**, *32*: 80-86.

[21] Martineau, R.L.; Anderson, C.A.; Smith, F.W. Expansion of Cylindrical Shells Subjected to Internal Explosive Detonations. *Exp. Mech.* **2000**, *20*: 219-225.

[22] Deng, H.; Quan, J.; Liang, Z. Influence of Eccentric Initiation on Energy Distribution Gain of a Warhead Charge. *Explos. Shock Waves* **2022**, *42*(5): paper 052201; https://doi.org/10.11883/bzycj-2021-0280.

[23] Miao, C.; Liang, Z.; Deng, D. Numerical Simulation Influence of Curvature Radius on Focusing Warhead. *Ordnance Industry Automation* **2018**, *37*: 93-96.

[24] Li, X.; Wang, W.; Liang, Z. Fragment Dispersion Characteristics of the "Cross-Shape" Built-in Fragmentation Directional Warhead. *Explos. Shock Waves* **2023**, *43*(6): 1-11.

[25] Gao, Y.; Feng, S.; Zhang, B. Effect of the Length-Diameter Ratio on the Initial Fragment Velocity of Cylindrical Casing. *IOP Conf. Ser. Mater. Sci. Eng.* **2019**, *629*: 12-20.